Journal of ELECTRONIC MATERIALS, Vol. 48, No. 9, 2019
https://doi.org/10.1007/s11664-019-07399-w

Structural and Thermoelectric Properties of Solid–Liquid In_4Se_3-In Composite

SON D.N. LUU ,[1] TARAS PARASHCHUK,[1] ARTUR KOSONOWSKI,[1,2] THANG B. PHAN,[3] and KRZYSZTOF T. WOJCIECHOWSKI[1,2,4]

1.—Centre of Thermoelectric Materials Research, The Lukasiewicz Research Network – The Institute of Advanced Manufacturing Technology, 37A Wroclawska, 30-011 Cracow, Poland. 2.—Thermoelectric Research Laboratory, Faculty of Materials Science and Ceramics, AGH University of Science and Technology, 30 Mickiewicza, 30-059 Cracow, Poland. 3.—Center for Innovative Materials and Architectures (INOMAR), Vietnam National University, Ho Chi Minh City 721337, Vietnam. 4.—e-mail: wojciech@agh.edu.pl

The aim of our work was to investigate thermoelectric properties of a composite of solid In_4Se_3 and solid or liquid indium. Polycrystalline In_4Se_3-In composites were prepared by a direct reaction of elements, powdering of products and sintering powders by pulsed electric current sintering technique. Microstructural and structural properties of obtained composites were analyzed using SEM + EDX and XRD techniques. Electrical transport properties and thermal conductivity were measured over a temperature range of 323 K ≤ T ≤ 673 K. Results show that the electrical conductivity of composite increases about four times in comparison with that of pristine In_4Se_3. The thermal conductivity decreases in a systematic way with the increase of In content and reaches a value of about 0.44 W m^{-1} K^{-1}. As a result, the addition of indium enhances the thermoelectric figure of merit ZT from 0.8 to 1.2 at 673 K. However, we found that the melting of indium at about 430 K has no significant influence on thermoelectric properties of composites. We assume that the improvement of electrical properties is mainly due to the formation of point defects in In_4Se_3 phase and metallic properties of the In phase. To analyze formation energies of possible defects in In_4Se_3 structure, DFT calculations within the molecular cluster model were carried out. It was found that the In interstitial atoms are energetically more favorable than the formation of Se vacancy in In_4Se_3 structure.

Key words: Thermal conductivity of In_4Se_3+In composite, thermoelectric figure of merit of In_4Se_3+In composite, metal-semiconductor, In_4Se_3

INTRODUCTION

Thermoelectric (TE) materials have attracted ever-increasing attention as sustainable and renewable energy resources.[1] The performance of TE material is determined by the dimensionless thermoelectric figure of merit, $ZT = S^2\sigma T/\kappa$, where S, σ, T and κ are the Seebeck coefficient, the electrical conductivity, the absolute temperature, and the thermal conductivity, respectively. In_4Se_3-based materials have been intensively investigated as the promising mid-temperature range TE material.[2,3] In_4Se_3 crystallizes in a layered orthorhombic structure with a space group of *Pnnm*. The $(In_3)^{5+}$ clusters are covalently bonded to Se^{2-} ions in the *b*-*c* plane whilst the van der Waals interaction connects the interlayers along the *a* axis.[2,4] The relatively strong interaction between the layers is created by interstitial In^+ ions, and thus enhancing its mechanical properties (Fig. 1). The thermoelectric

(Received January 31, 2019; accepted June 25, 2019; published online July 8, 2019)

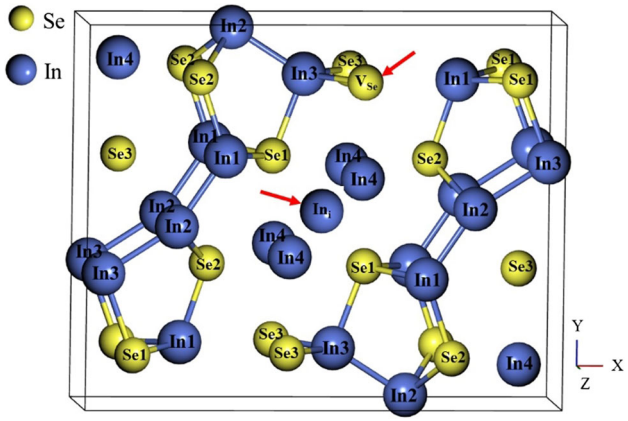

Fig. 1. The crystal structure of In_4Se_3. Arrows show the position of the considered defects: In interstitial defect and Se vacancy, respectively.

properties of *n*-type single crystal In_4Se_{3-x} was firstly reported with remarkable high ZT value of 1.48 at 705 K along the *b*-*c* plane.[2] During the last decade, efforts on improving the thermoelectric performance of this material have been continually increased. Through optimizing the carrier concentration and improving the carrier mobility by Cl doping, Rhyee et al. reported an enhanced ZT of 1.53 at 723 K.[5] However, the single crystal In_4Se_3 has drawbacks of strong anisotropy, poor mechanical properties, and high production cost. Therefore, more efforts on the development of high-performance polycrystalline In_4Se_3 as a replacement of single crystalline In_4Se_{3-x} has been actively invested.[6] Recently, thermoelectric properties of single and polycrystalline In_4Se_3 based materials have been reviewed in Refs. 4, 7, 8. Most of the TE properties of polycrystalline In_4Se_3 are usually enhanced by multi-element doping,[6,9,10] copper nano-inclusion,[11] copper interaction and bromine substitution at Se sites.[12] Very few investigations of thermoelectric properties of the In_4Se_3 composite have been carried out. For instance, the nano $SrTiO_3$ dispersed In_4Se_3/InSe composite shows a ZT of 0.2 at 600 K[13] while the composite of In_4Se_3 + 20 wt.% In_4Te_3 reported a ZT of 0.56 at 672 K.[14] Zhai et al. reported the thermoelectric properties of single crystal In_4Se_3-In composite using the zone melting method with a ZT of 0.9 (measured perpendicularly to growth direction) at 700 K.[15] The composite of $In_4Se_{2.7}Cl_{0.03}$-$BaIn_2Se_4$ shows an increase of Hall mobility and electrical conductivity of a sample.[16] The presence of metallic In in In_4Se_3 matrix was confirmed in other works.[17,18] However, the effect of In as the second phase on the thermoelectric properties of the In_4Se_3 matrix was not investigated sufficiently. Due to the low melting point of In, the In_4Se_3 composite with liquid In phase could be considered as a new type of thermoelectric material.

The thermal conductivity of composite materials can be strongly reduced by effective phonon scattering at the interfaces of two dissimilar materials while the work function of metal could result in the injection of electrons to the intrinsic host semiconductor.[19,20] Therefore, it is very interesting to investigate the thermoelectric properties of the semiconductor–metal composite. On the other hand, the selective scattering of low energy charge carriers at the metal–semiconductor interface, as a charge carrier filter, could produce the high Seebeck coefficient.[19,20] In addition, solid–solid and solid–liquid phase boundaries in the In_4Se_3–In system can have a significant influence on the transport of heat.

In this paper, the synthesis, characterization of structural and thermoelectric properties of semiconductor–metal In_4Se_3 + *x* wt.% In (*x* = 0; 3; 18) composites are presented. We suppose that the improvement of electrical properties is mainly due to the formation of point defects in In_4Se_3 phase and effects of metallic In phase. Therefore, the formation energy of possible defects in the In_4Se_3 structure was also calculated using the density functional theory (DFT) to determine their influence on the structural and electrical properties of In_4Se_3 phase.

EXPERIMENTAL

Synthesis and Characterization

The material was synthesized by direct reaction of elements in evacuated and sealed silica tubes from a mixture of In (99.99%, Alfa Aesar) and Se (99.5%, Alfa Aesar). The mixture of In_4Se_3 + *x* wt.% In (*x* = 0; 3; 18) components was first heated up to 573 K for 20 h and then up to 673 K for 12 h with a 0.5 K min^{-1} rate and cooled down in the furnace. Next, the materials were taken from the ampule, powdered by hand milling. Then, the powders were closed in a silica tube under vacuum again and annealed at 673 K for a further 10 h and then at 873 K for 5 h. After these procedures, the XRD analysis of products confirmed the presence mostly of In_4Se_3, InSe, and In phases. Finally, the material was milled again and annealed at 623 K for 120 h. Structural XRD analysis showed the presence of mainly In_4Se_3, and In phases.

Samples were characterized by powder x-ray diffraction (XRD) using the PANalytical Empyrean diffractometer, operating with $CuK_{\alpha 1}$ radiation (λ = 1.54056 Å). Data were collected over a range of $20 \le 2\theta/^\circ \le 70$, 0.022° step. Rietveld refinements were carried out using GSAS software.[21] Microstructural analysis was performed using the JEOL JSM-6460 LV scanning electron microscopy (SEM) while the composition of the sample was determined by the electron dispersive spectroscopy (EDS). The differential scanning calorimetry (DSC) was carried out using a Netzsch 404 F3 instrument. The sample was loaded into an aluminum crucible and heated from room temperature to 673 K, with a step of 5 K, under an Ar flow.

Compression Tests

Two cylindrical specimens of In_4Se_3 + 18 wt.% In with diameter of ~ 4.9 mm and height of ~ 5.9 mm and 6.9 mm, respectively, were axially compressed at room temperature with a speed of 1 mm/min using a universal testing machine Zwick/Roell Z150.

DFT Calculations

Calculations of defect formation energy of In in In_4Se_3 structure were performed using Firefly 8 package within the density functional theory formalism.[22] The convergence criteria for Self-Consistent Field (SCF) method calculations were chosen as $\Delta E_{SCF} = 10^{-4}$ eV. Calculations were carried within the Stevens–Basch–Krauss–Jasien–Cundari (SBKJC) parameterization.[23] The core states were calculated fully relativistically while the valence states were treated in a non-relativistic approach. DFT calculations performed by using Becke's three-parameter hybrid method[24] with the Lee, Yang and Parr (B3LYP) gradient corrected correlation functional.[25] A supercell model was not used, however, a cluster approach was done, where defects were directly arranged in the In_4Se_3 lattice. In our calculations, the cluster of In_4Se_3 contains 84 atoms and has a chemical formula $In_{48}Se_{36}$, which is equal to 12 formula units of In_4Se_3. Cluster models for calculations have been chosen according to In_4Se_3 crystal structure (Fig. 1) with experimental lattice parameters of a = 15.30 Å, b = 12.31 Å, c = 4.08 Å.[3]

Electrical and Thermal Transport Properties

For electrical and thermal conductivity measurements, the as-prepared powders were compacted by Pulsed Electric Current Sintering (PECS) technique at 673 K with a uniaxial pressure of 60 MPa for 10 min under an Ar (99.999%) atmosphere and slowly cooled down. The pressed samples had 98% of theoretical density which measured by Archimedes' method with water as a liquid. The obtained densities are comparable to those of calculations using geometrical parameters.

The electrical conductivity and Seebeck coefficient were measured by standard techniques using lab-built equipment under a vacuum environment (~ 10^{-2} torr) at a temperature range of 323 K ≤ T ≤ 673 K. The PECS-sintered samples with an approximate diameter of 5 mm and length of 12 mm were used to measure the electrical conductivity using a four-probe method with a DC power source. For the Seebeck coefficient measurement, an auxiliary heater was used to maintain a temperature gradient of 5 K between top and bottom of samples. Thermoelectric properties in heating and cooling cycles of three samples for each composition were also carried out (see the Fig. 8 and the supplementary Figure S3-S5). Thermal diffusivity (α) of the sample over the same temperature range in 50 K steps was measured by the LFA 457 MircoFlash apparatus (see the supplementary Figure S6). The PECS -sintered samples with a diameter of 10 mm and a thickness of ~ 1.8 mm were coated by graphite on the surface of a pellet. The thermal conductivity (κ) is calculated from the relationship $\kappa = \alpha C_p \rho$, where ρ is the sample density. The heat capacity (C_p) was measured by a Netzsch 204 F1 instrument. The electrical and thermal measurements were carried out in the direction parallel to the pressing force.

RESULTS AND DISCUSSION

Figure 2 shows the powder x-ray diffraction patterns of In_4Se_3 + x wt.% In (x = 0; 3; 18) samples. Analysis of these data indicates that the major phase is the orthorhombic In_4Se_3. The very small trace amount of InSe phase (less than ~ 1.4%) was noticed in these samples (Figs. 2, 3 and Table I), which should have negligible effect on properties of

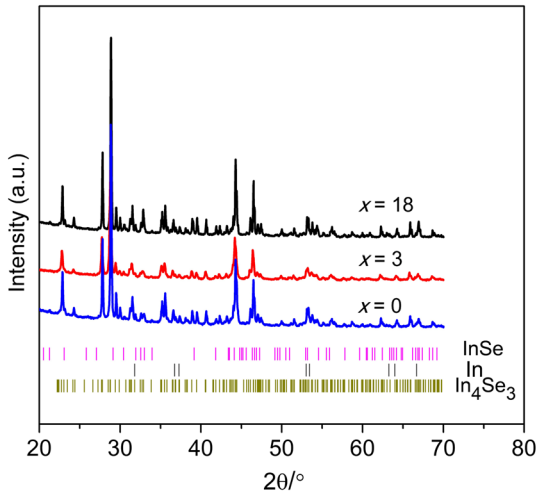

Fig. 2. X-ray diffraction patterns of In_4Se_3 + x wt.% In (x = 0; 3; 18).

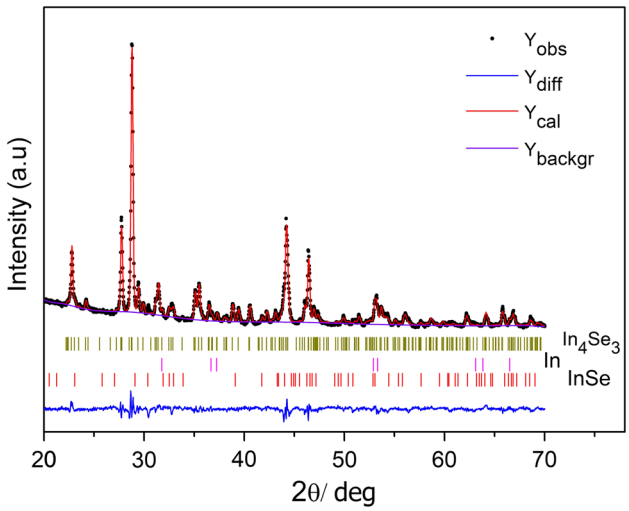

Fig. 3. Rietveld refinement using powder x-ray diffraction data for In_4Se_3 + 3 wt.% In.

Table I. Refined parameters for In_4Se_3 + x wt.% In (x = 0; 3; 18)

Nominal composition		x in In_4Se_3 + x wt.% In		
		0	3	18
In_4Se_3	a (Å)	15.2872 (6)	15.3011 (8)	15.2894 (5)
	b (Å)	12.3058 (4)	12.3169 (7)	12.3056 (8)
	c (Å)	4.0801 (8)	4.0840 (4)	4.0799 (2)
Calculated wt fraction In_4Se_3/InSe/In (%)		98.7/1.3/0.0	96.5/1.1/2.4	85.1/1.2/13.6
R_{wp} (%)		3.74	2.60	4.90

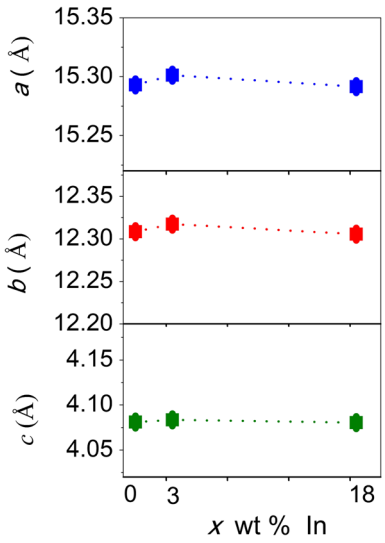

Fig. 4. Lattice parameters (a, b, and c) of In_4Se_3 + x wt.% In (x = 0; 3; 18).

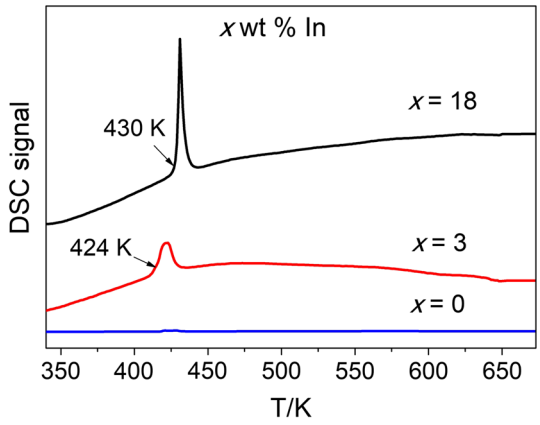

Fig. 5. The differential scanning calorimetry (DSC) curves of In_4Se_3 + x wt.% In (x = 0; 3; 18) with an evidence of endothermic peaks at 424 K (x = 3 wt.%) and 430 K (x = 18 wt.%), which are in good agreement with the melting point of In element (~ 430 K).

samples. A representative Rietveld refinement result is shown in Fig. 3. Other refinement results are presented in supplementary Figure S1-S2 and Table SI. The analysis of structural data shows that the lattice parameters of In_4Se_3 phase do not change (within the error magnitude) with the increased In amount (Fig. 4 and Table I). It indicates that possible deviation from stoichiometry is very small. This result is consistent with those of Osters et al.[26] The presence of In as the second phase in the In_4Se_3 matrix of composite samples was confirmed by DSC analysis (Fig. 5), and SEM + EDX observations (Fig. 6). The DSC results show an endothermic peak in In_4Se_3 + 18 wt.% In starting at 430 K, this is in excellent agreement with the melting point of indium (~ 429.6 K).[27] However, for the In_4Se_3 + 3 wt.% In sample, the In melting starts at 424 K. This can be explained by the presence of nano-size inclusions of indium. This suggestion is consistent with observations in Refs. 6 and 15.

The quantitative analysis (EDS) of In_4Se_3 + 3 wt.% In sample indeed confirms the precipitation of In as the second phase (Fig. 6 and Table II). Particularly, in Fig. 6, the In-rich region (R1) is surrounded by In_4Se_3 grains (R2-4) with almost the same chemical composition (Table II). This result is consistent with DSC measurement in which elemental In was detected in In_4Se_3 + x wt.% In (x = 0; 3; 18). Precise EDS analysis of chemical composition of various regions shows a slight deviation from the stoichiometry of In_4Se_3 in the direction of an excess of In ($In_{4+x}Se_3$—i.e., interstitial In) or deficiency of Se (In_4Se_{3-y}—i.e., vacancies in the Se sublattice). Despite a favorable type of defect, the deviation from stoichiometry is small (x, $y < 0.08$) which controverts to previous works.[2,9,18] For example, Rhyee et al. reported a single crystal $In_4Se_{2.35}$ could be obtained by the Bridgeman method[2] or Zhu et al., reported the success of synthesis of Se deficiency polycrystalline In_4Se_{3-x} compounds by ball milling and hot-pressing,[18] or Ann et al. reported the synthesis of cationic substitution on the thermoelectric properties of $In_{4-x}M_xSe_{2.95}$.[9]

Mechanical Strength

Compression tests show that the In rich In_4Se_3 + 18 wt.% In composite sample can withstand a maximum stress of 140 MPa and a Young's modulus of 840 MPa. Most TE materials have a fracture strength in the range of 60–200 MPa, depending on material and the testing method. For instance, the commercialized Bi_2Te_3 has a fracture strength of 62 MPa.[28] The skutterudites and half-Heuslter materials have higher strengths of 600–

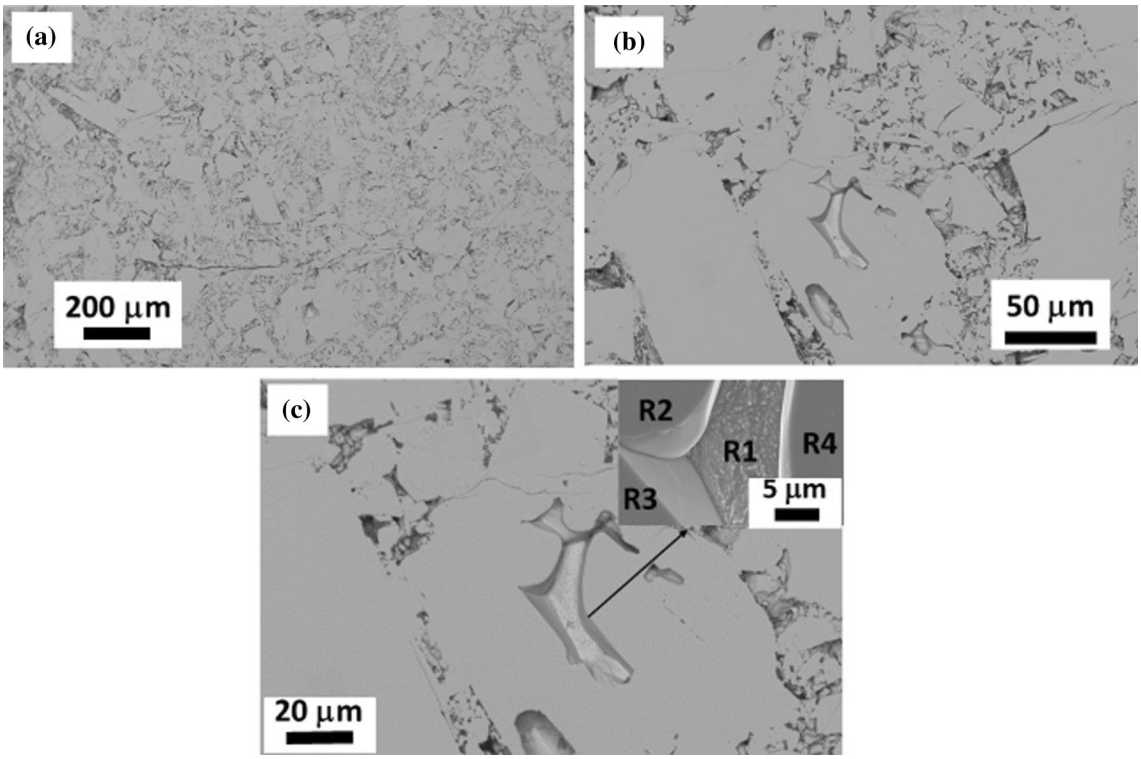

Fig. 6. SEM micrographs of PECS sintered In_4Se_3 + 3 wt.% In sample: (a) at 200μm; (b) at 50μm; (c) at 20μm. The inset of (c) shows four selected regions for EDS measurements.

Table II. EDS measurement of In_4Se_3 + 3 wt.% In sample (or nominal composition: $In_{4.138}Se_3$)

Region (R)	Se (% wt)	In (% wt)	Total (% wt)	Possible composition
R1	6.80	93.20	100	In_4Se_3 + InSe + In
R2	33.60	66.40	100	$In_{4.08}Se_3$ or $In_4Se_{2.94}$
R3	33.60	66.40	100	$In_{4.08}Se_3$ or $In_4Se_{2.94}$
R4	33.90	66.10	100	$In_{4.02}Se_3$ or $In_4Se_{2.98}$
Stoichiometric In_4Se_3	34.03	65.97	100	In_4Se_3

800 MPa.[29,30] The highest strength of a TE material has been addressed to MnSi with a strength of 1083 MPa.[31] It indicates that the In_4Se_3-In composites are usable for the TE applications.

Results of DFT Calculation

For prediction of the preferable type of defects in In_4Se_3 phase the ab initio calculation of defect formation energies have been performed. The defect formation energy E_{def} was calculated as follows:

$$E_{\mathrm{def}}(\mathrm{In}_i) = E(\mathrm{In}_{49}\mathrm{Se}_{36}) - E(\mathrm{In}_{48}\mathrm{Se}_{36}) - E(\mathrm{In}), \quad (1)$$

$$E_{\mathrm{def}}(V_{\mathrm{Se}}) = E(\mathrm{In}_{48}\mathrm{Se}_{35}) - E(\mathrm{In}_{48}\mathrm{Se}_{36}) + E(\mathrm{Se}), \quad (2)$$

where $E_{def}(In_i)$ and $E_{def}(V_{Se})$ are the formation energies of interstitial indium In_i and selenium vacancy V_{Se}, respectively. $E(In_{49}Se_{36})$, $E(In_{48}Se_{36})$ and $E(In_{48}Se_{35})$ are cluster energies. $E(In)$ and $E(Se)$ are energies of free atoms taken from the structure (V_{Se}) or added to structure (In_i), respectively.

According to Ref. 32, the most favorable position of Se vacancy is the Se_3 site (Fig. 1). Therefore, it was used for the DFT-calculations of the formation energy of the Se vacancy. In the In_4Se_3 lattice structure, one of the In sites is the cationic In_4 (4 g Wyckoff site) with + 1 valence state, and the other three In (1–3) are forming a trinuclear In_3^{5+} metallic bonding with + 5/3 valence state. According to Ref. 33, the substitutional atoms prefer In4 site than any other sites of In (1–3). This could be explained by the weaker Van der Waals interaction between layers comparing covalent bonds at trinuclear $(In_3)^{5+}(Se_3)^{6-}$ clusters. Therefore, in this calculation, the interstitial In was localized in the more favorable position between layers. The geometry optimization shows that an In atom occupies the interstitial positions without strong distortion of the defect vicinity. Such behavior of In atoms leads to the important conclusion about the possible

occupation of interstitial positions and their improvement of the electrical conductivity due to the contribution of an additional electron from each In atom into the structure. On the other hand, introducing more In atoms into In_4Se_3 structure could result in nano- and/or micro-inclusions. Calculations of defect formation energies, presented in Table III, clearly show that In interstitial defect is energetically more favorable than Se vacancy formation. It indicates that the structure prefers the interstitial position of In atoms in the In4 vicinity rather than to form a Se vacancy in $(In_3)^{5+}(Se_3)^{6-}$ clusters. These calculations strongly support our experimental results.

Thermoelectric Properties

The electrical conductivity of $In_4Se_3 + x$ wt.% In (x = 0; 3; 18) increases with the temperature rise, showing semiconducting behavior while negative Seebeck coefficient indicates that these materials are n-type semiconductors (Fig. 7). The electrical conductivity changes from the value of 1561 S m^{-1} (at 323 K) to 4113 S m^{-1} (at 673 K) for pristine In_4Se_3 (x = 0) or 1965 S m^{-1} (at 323 K) to 6282 S m^{-1} (at 673 K) and 2898 S m^{-1} (at 323 K) to 8417 S m^{-1} (at 673 K) for x = 3 wt.% and 18 wt.%, respectively. It was observed that the excess of In content significantly enlarges the electrical conductivity. Two factors can impact on this effect: (a) an increase of electrical conductivity of In_4Se_3 phase as the result of the increase of carriers concentration produced by point defects (In_i or V_{Se}) or (b) larger contribution in conductivity of metallic In phase in In_4Se_3–In composite. Indium is the metallic conductor while In_4Se_3 shows a semiconducting behavior in In_4Se_3–In composite. The contact of these two phases could result in electrons transfer from into In_4Se_3 to redistribute the charge carriers in this phase. In other words, the difference of the Fermi levels at metal–semiconductor junctions should result in electron diffusion.[34] However, with the current state of knowledge, it is hard to predict which type of carriers would be preferable. On the other hand, it is expected that the decrease of electrical conductivity after phase transition of indium would happen.[35] In our result, it does not show significant change after phase transition of indium. Therefore, we could assume that the effect of In liquid phase on the transport properties is not determinative. Furthermore, the semiconducting behavior of these composites suggests that electrical properties of materials are related to the zone before the percolation threshold for a metal—semiconductor composite. Therefore, the huge (almost twice) increase of electrical conductivity can be mainly the result of the carrier concentration increase in the In_4Se_3 phase. It should be mentioned that the temperature dependence of electrical conductivity changes its slope in all samples at high temperature, which could also indicate the influence of bipolar conduction in the In_4Se_3 phase.

Table III. Defect formation energy in In_4Se_3 lattice structure

Defect	Formation energy (eV)
Se vacancy	1.36
In interstitial	0.84

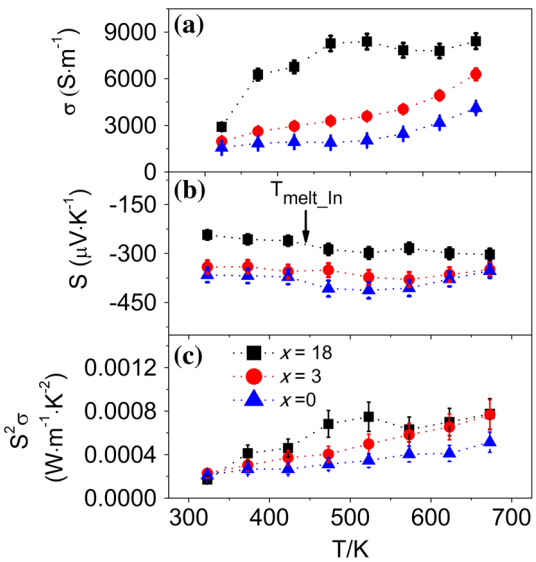

Fig. 7. Temperature dependence of electrical properties: (a) electrical conductivity (σ); (b) Seebeck coefficient (S); (c) power factor (σ^2·S) of $In_4Se_3 + x$ wt.% In (x = 0; 3; 18) at 323 K ≤ T ≤ 673 K.

The Seebeck coefficient S varies from − 366 μV/K (x = 0 wt.%) to − 243 μV/K (x = 18 wt.%) at 323 K, suggesting that the carrier concentration increases with the increase of In content. In general, the Seebeck coefficient value is inversely dependent to electrical conductivity, with an assumption that the electrical properties are determined by a carrier concentration.[36] However, in these composites, the absolute value of the Seebeck coefficient and electrical conductivity increases in parallel between 323 K and 573 K. This result might be related to the assumption of the filtering of low energy carriers at the interface barrier between In phase and In_4Se_3 matrix as suggested by some works.[19,37–39] Therefore, further systematic investigation of this phenomenon is desired. The bandgap for pristine In_4Se_3 was roughly estimated to be E_g = 0.43 eV, using the equation of

$$E_g = 2eS_{max}T_{max},$$

where e, S_{max}, T_{max} are the electron charge, the maximum Seebeck coefficient, and the corresponding temperature, respectively.[40] This result is in excellent agreement with the value of In_4Se_3 ($E_g \sim 0.43$ eV) reported in Refs. 17 and 41. The activation energy determined from the lnσ versus

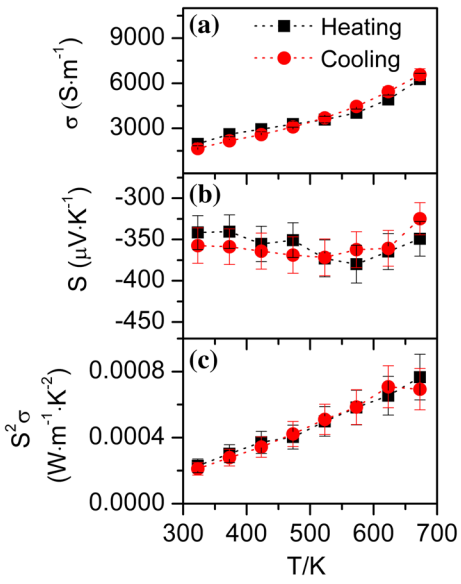

Fig. 8. Temperature dependence of electrical properties of heating and cooling cycles: (a) electrical conductivity (σ); (b) Seebeck coefficient (S); (c) power factor (σ^2·S) of In_4Se_3 + 3 wt.% In at 323 K ≤ T ≤ 673 K.

1/T was also used to estimate the band gap of In_4Se_3 at a temperature range of 523 K ≤ T ≤ 673 K (see Supplemental Figure S7), taking into account that for an intrinsic semiconductor $E_g = 2\,E_a$. The calculation shows that the bandgap of In_4Se_3 is ~ 0.4 eV which is comparable to the thermal band gap value estimated by the maximum Seebeck coefficient.

The power factor ($S^2\sigma$) of samples increases with increasing temperature, approaching a value of 0.51 mW m^{-1} K^{-2} (x = 0); 0.76 mW m^{-1} K^{-2} (x = 3 wt.%) and 0.77 mW m^{-1} K^{-2} (x = 18 wt.%) at 673 K, is comparable to those of In_4Se_{3-x} (~ 0.65 mW $m^{-1}K^{-2}$ at 700 K)[18] or $In_4Pb_{0.01}Sn_{0.03}Se_{2.5}$ (~ 0.75 mW m^{-1} K^{-2} at 700 K).[42] Comparing with stoichiometric In_4Se_3, the In_4Se_3-In composites have significantly enhanced values of power factor, which is important for the high performance of thermoelectric applications.

Figure 8 shows the thermoelectric properties in heating and cooling cycles of a representative sample of In_4Se_3 + 3% wt In. The thermoelectric data of other samples could be found in supplemental Figure S3-S4. Results show that samples are stable and reproductivity at the temperature range of 323 K ≤ T ≤ 673 K.

Thermal Properties

Table IV shows the temperature dependence of heat capacity for In_4Se_3 + x wt.% In (x = 0; 3; 18). These values are comparable to previous works.[18,43] Figure 9 shows the temperature dependence of thermal conductivity (κ) of In_4Se_3 + x wt.% In (x = 0; 3; 18) samples at a range of 323 K ≤ T ≤ 673 K. The contribution of electronic (κ_e) and lattice (κ_{lat}) thermal transports were estimated using the electrical conductivity data in conjunction with the Wiedemann–Franz law:

$$\kappa_e = L\sigma T, \tag{3}$$

where σ is the electrical conductivity, L is the Lorenz numberr. In fact, there is no already developed model for the estimation of Lorenz number for composites. Therefore, for a rough estimation of the contribution of the electronic part in heat transport, the value of L = 1.49 × 10^{-8} W Ω K^{-2} was used as for the nondegenerate semiconductor.[44–46]

Results show that the lattice thermal conductivities (or more precisely, the average transport of heat due to atom vibration in solid and liquid phases) of samples decrease in a systematic way

Table IV. Heat capacity C_p (J g K^{-1}) of In_4Se_3 + x wt.% In (x = 0; 3; 18) samples

	x in In_4Se_3 + x wt.% In		
Temperature (K)	**0**	**3**	**18**
323	0.256	0.252	0.262
373	0.261	0.255	0.268
423	0.262	0.257	0.271
473	0.262	0.257	0.271
523	0.261	0.258	0.272
573	0.262	0.259	0.274
623	0.264	0.261	0.277
673	0.271	0.267	0.281

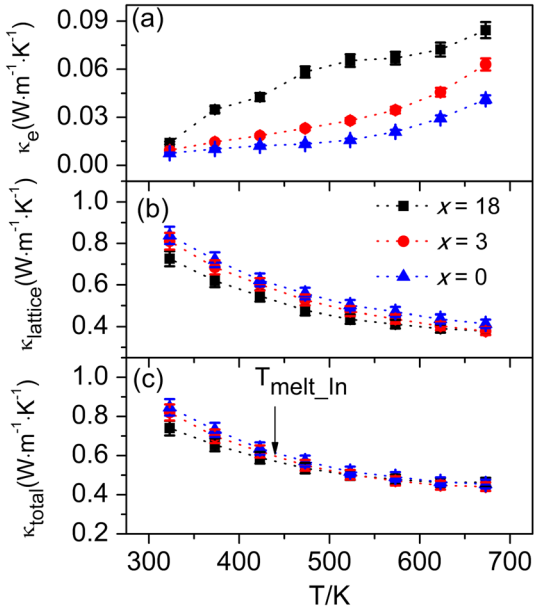

Fig. 9. Temperature dependence of (a) electronic thermal conductivity; (b) lattice thermal conductivity and (c) total thermal conductivity of In_4Se_3 + x wt.% In (x = 0; 3; 18) at a range of 323 K ≤ T ≤ 673 K.

with the increase of In content. In addition, the contribution of κ_{lat} dominates in all samples whilst that of κ_e is 0.9%; 1.2% and 1.9% of κ_{tot} at 323 K for x = 0 wt.%; 3 wt.%; and 18 wt.%, respectively. The electronic thermal contribution increases to 9.1%; 14.3% and 18.2% of κ_{tot} at 673 K for x = 0 wt.%; 3 wt.%; and 18 wt.%, respectively. It indicates that in In rich- In_4Se_3-In composite samples, this contribution is significant and proportional to the higher carrier concentration of the sample. The low thermal conductivity of these samples should be attributed by the phonon scattering at interlayers of their two-dimensional In/Se quasi-layers structures of In_4Se_3 phase, which is regularly found in natural 2D layer structures, for instance, SnSe[47] or LnOCuSe (Ln = La, Bi).[48–50] This low thermal conductivity might also result from phonon scattering at the phase boundary in composites,[51,52] from the point defects (In_i, V_{Se}) in the In_3Se_4, or other defects.[6,17,18] On the other hand, the additional effect of liquid–solid interphase at high temperature on the scattering of medium and high frequent phonons could also contribute to the low thermal conductivity of this composite. In fact, the indium melting during the measurement at high temperatures could result in the resistance of phonon propagation. The Debye temperature of single crystal In_4Se_3 was theoretically estimated with a value of 226 K and 239 K for a, b and c axis, respectively.[53] It suggests that the anharmonic lattice vibration could contribute to the temperature dependence of lattice thermal conductivity of In_4Se_3 with the increasing temperature. However, for metal—semiconductor composites, the temperature behaviour of thermal conductivity can be more complicated and related to the elastic properties of both materials. We plan to continue the research in this area in the future.

The figure of merit (ZT) of samples increases as a function of temperature (Fig. 10). The maximum ZT reaches to a value of 1.17 and 1.13 at 673 K for the sample of In_4Se_3 + 3 wt.% and 18 wt.% In, respectively. Given that the trend is increasing, the higher ZT would be expected at a higher temperature. However, according to thermal analyses, the maximum temperature should not be higher than 673 K because of the volatile Se. Therefore, this composite is suitable for thermoelectric application in the mid-temperature range. The enhanced electrical conductivity with moderate Seebeck coefficient and very low thermal conductivity result in good TE performance of In_4Se_3 + x wt.% In (x = 0; 3; 18) composite in comparison with the stoichiometric In_4Se_3, where ZT ~ 0.76 at 673 K. Our result is higher than those of several polycrystalline stoichiometric or doped In_4Se_3 materials.[9–15]

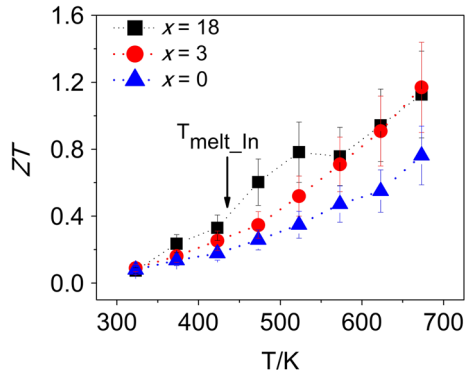

Fig. 10. Temperature dependence of figure of merit (ZT) of In_4Se_3 + x wt.% In (x = 0; 3; 18) at a range of 323 K ≤ T ≤ 673 K.

CONCLUSIONS

The composite of In_4Se_3 + x wt.% In (x = 0; 3; 18) was successfully synthesized via direct reaction of elements. We obtained unique liquid–solid composite material on the basis of liquid In and solid In_4Se_3 in which specific transport phenomena could occur. It was observed that the direct effect of metallic liquid In on the electrical conductivity is not significant, because the amount of this element could be lower than the value of the percolation threshold. However, the excess of In can produce an additional effect on the structural properties of In_4Se_3 phase. The experimental results and DFT calculations confirm that the formation of Se vacancy is less preferable in the In_4Se_3 structure when the In excess is introduced to the stoichiometric composition of In_4Se_3. The In atoms could rather occupy an interstitial position in the In^{1+} vicinity to provide more electrons in the In_4Se_3 matrix or formation of nano-micro inclusions and phase separation. Therefore, defects are playing a role of source of additional charge carriers in the In_4Se_3 phase. On the other hand, the formation of In phase in the In_4Se_3 matrix could also be a source of electrons due to the difference in Fermi levels in both phases. The similar mechanism has been proposed for the explanation of thermal conductivity behaviour.[54,55] It could be explained by two reasons: phonon scattering at phase boundaries of the metal In—semiconductor In_4Se_3 composition in solid–solid or solid–liquid state, and the second reason could be the result of the phonons scattering at point defects: In_i and V_{Se}.

The composition of the In_4Se_3–In composites has a higher electrical conductivity and lower thermal conductivity than those of pristine In_4Se_3 which allows us to obtain excellent enhancement of the thermoelectric figure of merit. The ZT parameter of 1.17 and 1.13 at 673 K is achieved for the composite of In_4Se_3 + 3 wt.% and 18 wt.% In, respectively, higher than that of the pristine In_4Se_3, ZT = 0.76 at the same temperature. The analyses of the possible reasons for increasing the ZT parameter obtained in this paper requires additional investigations, which is our aim for the next research.

ACKNOWLEDGMENTS

The "New approach for development of efficient materials for direct conversion of heat into electricity project" is carried out within the TEAM – TECH0076 program of the Foundation for Polish Science co-financed by the European Union under the European Regional Development Fund, and the beneficiary of this project is The Lukasiewicz Research Network – The Institute of Advanced Manufacturing Technology in Krakow (Poland).

ELECTRONIC SUPPLEMENTARY MATERIAL

The online version of this article (https://doi.org/10.1007/s11664-019-07399-w) contains supplementary material, which is available to authorized users.

REFERENCES

1. D.M. Rowe, *Renew. Energy* 16, 1251 (1999).
2. J.S. Rhyee, K.H. Lee, S.M. Lee, E. Cho, S.I. Kim, E. Lee, Y.S. Kwon, J.H. Shim, and G. Kotliar, *Nature* 459, 965 (2009).
3. J.H.C. Hogg, H.H. Sutherland, and D.J. Williams, *Acta Crystallogr. B* 29, 1590 (1973).
4. G. Han, Z.-G. Chen, J. Drennan, and J. Zou, *Small* 14, 2747 (2014).
5. J.S. Rhyee, K. Ahn, K.H. Lee, H.S. Ji, and J.H. Shim, *Adv. Mater.* 23, 2191 (2011).
6. Z.S. Lin, L. Chen, L.M. Wang, J.T. Zhao, and L.M. Wu, *Adv. Mater.* 25, 4800 (2013).
7. J.S. Rhyee and J.H. Kim, *Mater* 8, 1283 (2015).
8. X. Yin, J.-Y. Liu, L. Chen, and L.-M. Wu, *Acc. Chem. Res.* 51, 240 (2018).
9. K. Ahn, E. Cho, J.S. Rhyee, S.I.I. Kim, S.M. Lee, and K.H. Lee, *Appl. Phys. Lett.* 99, 102110 (2011).
10. Y.S. Lim, M. Jeong, W.S. Seo, J.H. Lee, C.H. Park, M. Sznajder, L.Y. Kharkhalis, D.M. Bercha, and J.H. Yang, *J. Phys. D* 46, 275304 (2013).
11. G. Li, J.Y. Yang, Y.B. Luo, Y. Xiao, L.W. Fu, M. Liu, and J.Y. Peng, *J. Am. Ceram. Soc.* 96, 2703 (2013).
12. Y.B. Luo, J.Y. Yang, G. Li, M. Liu, Y. Xiao, L.W. Fu, W.X. Li, P.W. Zhu, J.Y. Peng, S. Gao, and J.Q. Zhang, *Adv. Energy Mater.* 4, 1300599 (2014).
13. M.H. Lee, J.S. Rhyee, M. Vaseem, Y.B. Hahn, S.D. Park, H.J. Kim, S.J. Kim, H.J. Lee, and C. Kim, *Appl. Phys. Lett.* 102, 223901 (2013).
14. J.Y. Cho, Y.S. Lim, S.-M. Choi, K.H. Kim, W.-S. Seo, and H.-H. Park, *J. Electron. Mater.* 40, 1024 (2011).
15. Y.B. Zhai, Q.S. Zhang, J. Jiang, T. Zhang, Y.K. Xiao, S.H. Yang, and G.J. Xu, *J. Mater. Chem. A* 1, 8844 (2013).
16. J.H. Kim and J.-S. Rhyee, *Electron. Mater. Lett.* 10, 801 (2014).
17. P.K. Rawat, H. Park, J. Hwang, and W. Kim, *J. Elec. Mat.* 46, 3 (2017).
18. G.H. Zhu, Y.C. Lan, H. Wang, G. Joshi, Q. Hao, G. Chen, and Z.F. Ren, *Phys. Rev. B* 83, 115201 (2011).
19. S.V. Faleev and F. Léonard, *Phys. Rev. B* 77, 214304 (2008).
20. M. Zebarjadi, G. Joshi, G. Zhu, B. Yu, A. Minnich, Y. Lan, X. Wang, M. Dresselhaus, Z. Ren, and G. Chen, *Nano Lett.* 11, 2225 (2011).
21. B.H. Toby and R.B.V. Dreele, *J. App. Cryst.* 46, 544 (2013).
22. A. Granovsky, PC GAMESS version 7.0, http://classic.chem.msu.Su/gran/gamess/index.html.
23. W.J. Stevens, H. Basch, and M. Krauss, *J. Chem. Phys.* 81, 6026 (1984).
24. A.D. Becke, *J. Chem. Phys.* 98, 1372 (1993).
25. C. Lee, W. Yang, and R.G. Parr, *Phys. Rev. B.* 37, 785 (1988).
26. O. Osters, G. Blazek, and T. Nilges, *Z. Anorg. Allg. Chem* 639, 497 (2013).
27. A. John, *Dean (523), Lange's handbook of chemistry*, 15th ed. (New York: McGraw-Hill Inc, 1999), p. 1128.
28. L.-D. Zhao, B.-P. Zhang, J.-F. Li, M. Zhou, W.-S. Liu, and J. Liu, *J. Alloys. Comps.* 455, 259 (2008).
29. V. Ravi, S. Firdosy, and T.Caillat, in *L.B. Conference, AIP Conference* (2008).
30. P. Le, C.-W. Luo, S.-R. Jian, T.-C. Lin, and P.-F. Yang, Mater. *Chem. Phys.* 182, 72 (2016).
31. Y. Gelbstein, J. Tunbridge, R. Dixon, M. Reece, H. Ning, and R. Glchrist, et al., *J. Elect. Mat.* 43, 1703 (2014).
32. D.B. Luo, H.G. Si, and Y.X. Wang, *J. Alloy. Comp.* 589, 125 (2014).
33. A.S. Abhari, M. Abdellahi, and M. Bahmanpour, Ceram. *Int.* 42, 5593 (2016).
34. Y. Liu, D. Cadavid, M. Ibáñez, S. Ortega, S. Martí-Sánchez, O. Dobrozhan, M.V. Kovalenko, J. Arbiol, and A. Cabot, *APL Mater.* 4, 104813 (2016).
35. H.A. Davies and J.S. Llewelyn Leach, *Phys. Chem. Liq.* 2, 1 (1970).
36. G.J. Snyder and S.E. Toberer, *Nat. Mater.* 7, 105 (2008).
37. J. Martin, L. Wang, L.D. Chen, and G.S. Nolas, *Phys. Rev. B Condens. Matter Mater. Phys.* 79, 115311 (2009).
38. B. Moyzhes and V. Nechinsky, *Appl. Phys. Lett.* 73, 1895 (1998).
39. M.O. Zide, J.-H. Bahk, R. Singh, M. Zebarjadi, G. Zeng, H. Lu, J.P. Feser, D. Xu, S.L. Singer, Z.X. Bian, A. Majumdar, J.E. Bowers, A. Shakouri, and A.C. Gossard, *J. Appl. Phys.* 108, 123702 (2010).
40. H.J. Goldsmid and J.W. Sharp, *J. Electron. Mater.* 28, 869 (1999).
41. X. Shi, J.Y. Cho, R. Savador, J. Yang, and H. Wang, *Appl. Phys. Lett.* 96, 162108 (2010).
42. J.H. Kim, M.J. Kim, S. Oh, and J.S. Rhyee, *J. Alloy. Comp.* 615, 933 (2014).
43. K. Ahn, E. Cho, J.S. Rhyee, S. Kim, S. Hwang, H.-S. Kim, S.M. Lee, and K.H. Lee, *J. Mater. Chem.* 22, 5730 (2012).
44. P. Price, *IBM J. Res. Dev.* 1, 147 (1957).
45. H.-S. Kim, Z.M. Gibbs, Y. Tang, H. Wang, and G.J. Snyder, *APL Mater.* 3, 041506 (2015).
46. M. Thesberg and H. Kosina, N. Neophytou. *Phys. Rev. B* 95, 125206 (2017).
47. L.-D. Zhao, S.-H. Lo, Y. Zhang, H. Sun, G. Tan, C. Uher, C. Wolverton, V.P. Dravid, and M.G. Kanatzidis, *Nature* 508, 373 (2014).
48. M.L. Liu, L.B. Wu, F.Q. Huang, L.D. Chen, J.A. Ibers, and J. Solid, State. *Chem.* 180, 62 (2007).
49. H. Hiramatsu, H. Yanagi, T. Kamiya, K. Ueda, M. Hirano, and H. Hosono, *Chem. Mater.* 20, 326 (2008).
50. S.D.N. Luu and P. Vaqueiro, *J. Mater. Chem. A* 1, 12270 (2013).
51. D.J. Bergman and L.G. Fel, *J. Appl. Phys.* 85, 8205 (1999).
52. H. Xie, X. Su, Y. Yan, W. Liu, L. Chen, J. Fu, J. Yang, C. Uher, and X. Tang, *NPG Asia Mater.* 9, e390 (2017).
53. H.S. Ji, H. Kim, C. Lee, J.-S. Rhyee, M.H. Kim, M. Kaviany, and J.-H. Shim, *Phys. Rev. B* 87, 125111 (2013).

54. H. Xie, X. Su, Y. Yan, W. Liu, L. Chen, J. Fu, J. Yang, C. Uher, and X. Tang, *NPG Asia Mater.* 9, e390 (2017).
55. D.J. Bergman and L.G. Fel, *J. Appl. Phys.* 85, 8205 (1999).